PHYSICAL REVIEW D **86,** 062001 (2012)

Polarization speed meter for gravitational-wave detection

Andrew R. Wade,[1] Kirk McKenzie,[2] Yanbei Chen,[3] Daniel A. Shaddock,[1] Jong H. Chow,[1] and David E. McClelland[1]

[1]*Centre for Gravitational Physics, Department of Quantum Science, The Australian National University, Canberra, ACT, 0200, Australia*
[2]*Jet Propulsion Laboratory (JPL), California Institute of Technology, 4800 Oak Grove Drive, Pasadena, California 91109, USA*
[3]*Theoretical Astrophysics 350-17, California Institute of Technology, Pasadena, California 91125, USA*

(Received 21 May 2012; published 5 September 2012)

We propose a modified configuration of an advanced gravitational-wave detector that is a speed-meter-type interferometer with improved sensitivity with respect to quantum noise. With the addition of polarization-controlling components to the output of an arm cavity Michelson interferometer, an orthogonal polarization state of the interferometer can be used to store signal, returning it later with opposite phase to cancel position information below the storage bandwidth of the opposite mode. This modification provides an alternative to an external kilometer-scale Fabry-Pérot cavity, as presented in earlier work of Purdue and Chen [Phys. Rev. D **66**, 122004 (2002)]. The new configuration requires significantly less physical infrastructure to achieve speed meter operation. The quantity of length and alignment degrees of freedom is also reduced. We present theoretical calculations to show that such a speed meter detector is capable of beating the strain sensitivity imposed by the standard quantum limit over a broad range of frequencies for Advanced Laser Interferometer Gravitational-wave Observatory-like parameters. The benefits and possible difficulties of implementing such a scheme are outlined. We also present results for tuning of the speed meter by adjusting the degree of polarization coupling, a novel possibility that does not exist in previously proposed designs, showing that there is a smooth transition from speed meter operation to that of a signal-recycling Michelson behavior.

DOI: 10.1103/PhysRevD.86.062001 PACS numbers: 04.80.Nn, 03.67.-a, 95.55.Ym

I. INTRODUCTION

Gravitational-wave (GW) detectors, such as Advanced Laser Interferometer Gravitational-wave Observatory (Adv. LIGO), are Michelson-like interferometers designed to detect strains of 10^{-23} or less [1]. One contributing noise source limiting the sensitivity of these instruments is the quantum fluctuations in their light fields, also known as quantum noise, that imposes a theoretical limit to their sensitivity known as the standard quantum limit (SQL) [2]. This limit applies to nonresonant Michelson detectors and is imposed by the compromise between laser shot noise and radiation pressure noise that results from photon recoil off mirrors. Radiation pressure noise is expected to dominate at low frequencies and is a kind of measurement back action that limits the sensitivity of the instrument. Various schemes have been investigated with the express aim of circumventing the SQL [2–8].

This paper explores a theoretical speed meter configuration that is a relatively minor modification to the proposed advanced interferometer configurations, such as the Adv. LIGO, Virgo and KAGRA [1,9,10]. The configurations explored in this paper are proposed as third generation concepts for these instruments. With the addition of polarization optics, light may be stored on a second polarization of the interferometer before being returned with opposite phase to cancel position signals below the bandwidth of the opposite polarization storage mode. This design was inspired by a speed meter topology proposed by Purdue and Chen [11] that used an external four-kilometer Fabry-Pérot (FP) cavity to provide position signal cancellation. An alternative speed meter configuration, using polarization, was previously proposed by Danilishin [12] that replaced the Michelson beam splitter with a polarizing beam splitter and placed quarter-wave plates in the arms to couple the two arm cavity modes. In the scheme presented here quarter-wave plates are removed to the output to avoid having to pass large circulating power, and a linear orthogonal polarization is used as a storage mode. An advantage of the design proposed here is that the existing infrastructure of the LIGO interferometers would require minimal modification with changes only to the output optics and the Michelson beam splitter.

A speed meter interferometer is a device that measures the relative velocity of test masses instead of relative position. This is achieved by sampling the test mass position twice, cancelling position signals and modifying the reactance of test mass to amplitude quadrature fluctuations in the light field. The result is an interferometer that has a strain signal response proportional to frequency and a test mass response to amplitude quadrature vacuum fluctuations that is constant in frequency. The recoil of test masses to amplitude fluctuations leads to correlations forming from the amplitude quadrature into the phase quadrature. For speed meters, this response is constant in magnitude as a function of frequency. Thus its contribution to quantum noise competing with the GW signal will be cancelled with the correct choice of homodyne readout angle. Speed meters are a type of quantum nondemolition scheme that can circumvent back action noise, allowing measurement below the SQL over a broad range of frequencies.

We first describe the operation of the polarization speed meter and sketch a mathematical description of its operation. We show that, in the absence of other noise sources, such a speed meter detector is capable of beating the strain sensitivity limit imposed by the SQL over a broad frequency range. We also show how a small variation in this design, involving adjustment of polarization coupling by rotation of a wave plate, can be used to tune a speed meter. This results in a smooth transition from speed meter operation to that of a signal-recycling Michelson behavior. Finally, we report on the possible sensitivity improvements achievable with this configuration for Advanced LIGO-like parameters and discuss the implementation for a kilometer-scale detector of this kind.

II. POLARIZATION CONFIGURATION CONCEPT AND THE MATHEMATICAL DESCRIPTION

A. The proposed polarization-folded speed meter

The proposed polarization-folded speed meter is illustrated in Fig. 1. This interferometer configuration is based on the advanced topologies of LIGO, Virgo and KAGRA [1,9,10] but with the addition of a quarter-wave plate and output coupling mirror as well as ancillary polarization readout optics. The advanced interferometer configuration (dashed box, Fig. 1) consists of an arm cavity power-recycled Michelson interferometer held to its dark fringe for destructive interference at the output (quadrature fields f_i'). In the absence of arm length modulations, injected laser light on the horizontal polarization is returned along its path of incidence. When a GW differentially modulates the arm lengths, phase modulation sidebands are generated that constructively interfere at the output side of the beam splitter. Thus, gravitational-wave signals are generated in the phase quadrature of the horizontal field at the output (f_i') by differential motion of end test masses.

In advanced configuration topologies power recycling and signal extraction mirrors are included to resonantly couple carrier light in and signal sidebands out of the arm cavities: these are omitted in this paper for the sake of simplifying the analysis of speed meter operation. The high circulating cavity power is similar to the 800 kW expected to be implemented in Advanced LIGO [13], and the large laser power required can be reduced by reintroducing a power recycling mirror. Here we principally concern ourselves with fixing arm cavity circulating power and understanding the dynamics of the system.

The purpose of the additional polarization optics at the output of the arm cavity Michelson is to couple signal and noise sideband fields to an orthogonal polarization mode of the Michelson interferometer. The output mirror and quarter-wave plates are a short distance from the Michelson beam splitter compared to the kilometer scale of the detector arms. Horizontally polarized signal and noise fields, reflected by the output coupler mirror, double pass through the quarter-wave plate, delaying one optical axis by half a wavelength. When the wave plate slow axis is oriented at 45°, the polarization of the light is rotated by 90° to the vertical and on this mode is coupled back into the interferometer. On this vertical polarization the light is

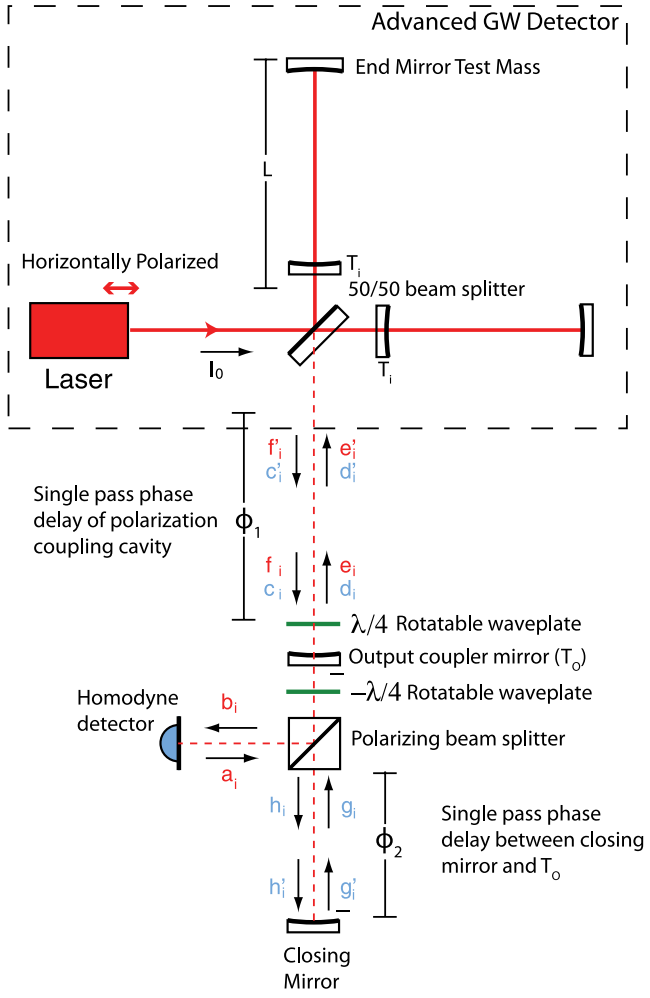

FIG. 1 (color online). Schematic of the polarization speed meter configuration. Horizontal linear polarization fields a, b, e and f and vertical fields c, d, g and h are indicated in red and blue respectively. Arm cavities are formed between the test mass mirrors and the arm cavity mirrors T_i, photons undergo a number of round trips, increasing their response to changes in the optical path due to GW. Carrier laser light is injected into the left port of the configuration in the horizontal polarization where the Michelson is held to its dark fringe on transmission. Differential test mass motion generates phase modulation sidebands in the horizontal polarization at the quadrature field point f_i'. The quarter-wave plate ($\lambda/4$) and output coupler mirror (T_o) couple these signals into an orthogonal polarization so that stored signals may couple back π out of phase to cancel position signals below the bandwidth of the polarization storage. The polarizing beam splitter isolates the two polarizations from each other so that the vertical polarization port can be closed with a mirror to prevent vacuum noise coupling in, and signals may be read out on the horizontal port only. The horizontal polarization is detected with a homodyne detector.

unaffected by modulations in end mirror position. In the absence of carrier light on the vertical mode, periodic changes in arm length do not pump coherent carrier light into signal and noise sidebands, and sidebands generated from signal and noise sidebands are negligibly small. Thus sidebands are stored on an orthogonal polarization in what is effectively a two-mirror cavity. Signals stored in the opposite polarization couple back π out of phase to cancel sidebands below the bandwidth of the orthogonal storage mode, canceling position information. The remaining phase modulations are due to velocity and higher order derivatives of position. The design invites direct comparisons to speed meter topologies previously proposed by Purdue and Chen [11] in which the orthogonal mode storage is instead provided by an external FP cavity. The equivalence between these two configurations is that the external FP cavity is now folded into an orthogonal mode of the Michelson interferometer. With the addition of polarization optics at the output an additional kilometer-scale external cavity and associated infrastructure are not needed.

B. Mathematical description of interferometer

Vacuum fluctuations in the electromagnetic fields couple in from open ports and points of loss in the system. In this analysis we consider the disturbance to the test masses by the open detector ports only.

In order to compute the strain sensitivity performance of the interferometer, it is first necessary to calculate the whole system input-output transfer function. This quantum transfer function expresses the output quadrature fields, (b_i) at the output detection port, in terms of the vacuum quadrature fields (a_i) coupled in from the open detection port and the gravitational strain "h" that is pumped from the carrier light field by modulation of the optical path. This relationship is found by solving the set of simultaneous equations including mirror junction conditions and linking free space propagation equations. For an interferometer held on its dark fringe and driven with a carrier field in the cosine quadrature and with arm cavities and output cavity held on resonance with the carrier, the transfer function takes the form

$$\begin{bmatrix} b_1 \\ b_2 \end{bmatrix} = e^{2i\beta}\begin{bmatrix} 1 & 0 \\ -\kappa & 1 \end{bmatrix}\begin{bmatrix} a_1 \\ a_2 \end{bmatrix} + \sqrt{2\kappa}e^{i\beta}\frac{h}{h_{\mathrm{SQL}}}\begin{bmatrix} 0 \\ 1 \end{bmatrix}, \tag{1}$$

where a_i and b_i are the quadrature fields as labeled in Fig. 1, and including the gravitational-wave strain signal h encoded in the phase quadrature. Here β is the overall sideband phase accrued and κ is the frequency-dependent radiation pressure coupling function of the system. Quantum noise in the interferometer output quadrature fields results from fluctuations of the input quadrature fields a_i. In the first term of Eq. (1), κ represents the strength of correlations from the amplitude to phase quadratures due to the recoil of photons off test masses. The second $\sqrt{\kappa}$ term is proportional to the amplitude of the carrier beam that is pumped into the phase quadrature by modulations of arm optical paths from gravitational waves. The factor $h_{\mathrm{SQL}} = \sqrt{8\hbar/m\Omega^2L^2}$ is the single-sided standard quantum limit that is factored out for convenience: this term represents the highest strain-referenced sensitivity for a nonresonant Michelson detector. Thus Eq. (1) represents a generic input-output transfer function for a nonresonant detector and is wholly characterized by the two principle quantities β and κ. By carefully engineering their form, one can determine the characteristic response and sensitivity performance of such a detector.

For speed meter operation the function κ should be constant over a broad range of frequencies. This is so that the signal response is linear in frequency. In this regime a homodyne readout quadrature angle φ can be chosen to measure $b_\varphi = b_1\cos(\varphi) + b_2\sin(\varphi)$ such that the strain equivalent quantum noise contribution is

$$h_n = \frac{h_{\mathrm{SQL}}}{\sqrt{2\kappa}}e^{i\beta}[a_1(\cot\varphi - \kappa) + a_2]. \tag{2}$$

For the correct choice of φ, where $\kappa(\Omega = 0) = \cot\varphi$, contributions to the quantum noise floor from the amplitude quadrature are canceled for a broad set of frequencies. This is not the case in position-like measurements for the unmodified advanced configuration where κ is a function of frequency. In that case, back action contributions from amplitude fluctuations (a_1) in the light field can only be minimized at select frequencies.

To solve the quantum transfer function for the configuration illustrated in Fig. 1, we must solve the simultaneous equations linking light fields along the propagation path of the vacuum fields. For an arm cavity Michelson the output quadrature fields (f_i), in terms of input quadrature fields (e_i) on the horizontal polarization, are as outlined by Kimble *et al.* [4] (see Fig. 1 for fields),

$$\begin{bmatrix} f_1 \\ f_2 \end{bmatrix} = e^{2i\alpha}\begin{bmatrix} 1 & 0 \\ -\mathcal{K} & 1 \end{bmatrix}\begin{bmatrix} e_1 \\ e_2 \end{bmatrix} + \sqrt{2\mathcal{K}}e^{i\alpha}\frac{h}{h_{\mathrm{SQL}}}\begin{bmatrix} 0 \\ 1 \end{bmatrix}, \tag{3}$$

where $\mathcal{K} = (2(I_0/I_{\mathrm{SQL}})\gamma^4)/(\Omega^2(\gamma^2 + \Omega^2))$ is the radiation pressure-driven coupling function of the arm cavity Michelson and $\alpha = \arctan\Omega/\gamma$ is the phase accrued by sidebands at GW frequency Ω reflected off each of the FP arm cavities. Here, γ is the bandwidth of each arm cavity. I_0 and I_{SQL} are the carrier laser power in the arms and laser power required to reach the SQL in a non-signal recycled interferometer, respectively. The form of these equations is identical to Eq. (3); however, in this case $\mathcal{K}$ is frequency-dependent. Because there is no injected coherent light on the vertical polarization, quadrature components of the field have nothing to beat against and $\mathcal{K}$ (for the vertical polarization) is zero. Thus the output fields (d_i) expressed in terms of the input fields (c_i) are

$$d_1 = e^{i2\alpha} c_1, \tag{4}$$

$$d_2 = e^{i2\alpha} c_2. \tag{5}$$

The quadrature fields are reflected with the same fixed phase delay α as the horizontal polarization. It is also necessary to take into account the evolution of the fields as they propagate between optics. Details are given in the Appendix, where Eqs. (A8) and (A9) may be applied for the propagation between the points f_i, d_i, e_i, c_i and f_i', d_i', e_i', c_i' as labeled in Fig. 1. Here the phase evolution of the fields is broken into a side band phase, $\phi_j = \Omega L/c$, proportional to the side band frequency Ω, arm length L and speed of light c, and a carrier phase $\Phi_j = \omega L/c$, proportional to the carrier frequency ω, which rotates the basis of the quadratures. Assuming that length scales to and from the polarization optics are negligible, then sideband phases accrued over these paths are $\phi_1 = \phi_2 \approx 0$. Additionally, absolute length is set to an integral and half integral numbers of wavelength such that $\Phi_1 = 0$ and $\Phi_2 = \pi/2$.

For the quarter-wave plate oriented at 45° to the horizontal, light is rotated 90° upon reflection. On transmission a second quarter-wave plate is oriented 90° to the first wave plate to cancel the rotation on transmission. The resulting junction conditions at the output coupler mirror, of transmittance T_0, are

$$e_i = \sqrt{T_o} a_i + \sqrt{1 - T_o} c_i, \tag{6}$$

$$d_i = \sqrt{T_o} g_i + \sqrt{1 - T_o} f_i, \tag{7}$$

$$h_i = \sqrt{T_o} c_i - \sqrt{1 - T_o} a_i, \tag{8}$$

$$b_i = \sqrt{T_o} f_i - \sqrt{1 - T_o} g_i. \tag{9}$$

Finally, a closing mirror is necessary in order to prevent vacuum field coupling in from the additional vertical open port. The closing mirror is assumed to be perfectly reflective so that $g_i' = -h_i'$.

We solve for the output quadrature fields b_i in terms of input vacuum fluctuations a_i and the GW strain h. A solution for quadrature fields b_i was found in the form of Eq. (3). The exact algebraic form for β and κ is cumbersome and the analytic expressions are not presented here. The noise spectral density is computed by setting the signal equal to noise and finding the corresponding square root of the spectral density as outlined by Buonanno and Chen [5]. The resulting coupling factor κ and strain equivalent sensitivity curve are presented in Figs. 2 and 3, respectively,

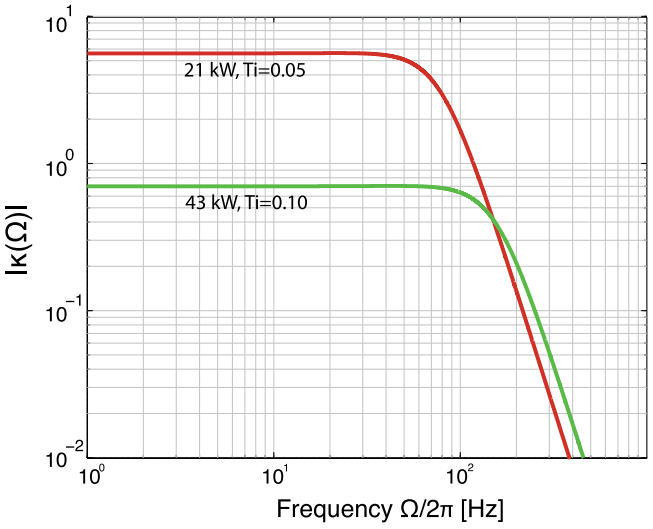

FIG. 2 (color online). Plot of the amplitude of the radiation pressure coupling function, κ, as a function of frequency. This shows a constant degree of coupling from the amplitude to the phase quadrature for frequencies up to 100 Hz. Below this bandwidth a homodyne readout angle may be chosen that projects out noise contribution from the amplitude quadrature. This plot is produced from the parameters presented in Table I with two choices of arm cavity finesse set by a T_i of 0.10 and 0.05. Circulating power was fixed at 850 kW with the power at the beam splitter adjusted for each of the T_i. Labels on curves indicate the beam splitter power and arm cavity mirror transmissivity.

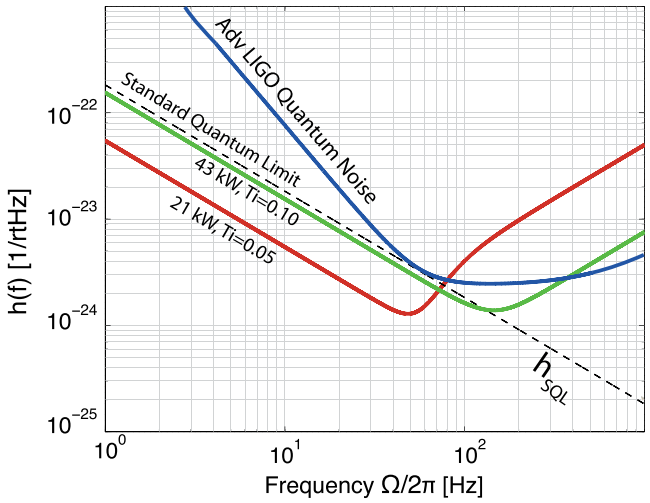

FIG. 3 (color online). Strain-equivalent quantum noise contribution as a function of frequency for the polarization-folded speed meter. Here three curves are displayed: two for the different choices of arm cavity mirror transmissivity $T_i = 0.10$ and $T_i = 0.05$ and a third that is the Advanced LIGO quantum noise contribution calculated using the software package GWINC [14]. Labels on curves indicate the choice of T_i and the beam splitter power to ensure circulating power at 850 kW. Also, for the polarization speed meter calculations, the homodyne readout phase has been adjusted to cancel amplitude quadrature contributions to the noise. It is shown here that the configuration can match the SQL using the parameters presented in Table I over a broad range of frequencies. Over a narrower range operation ($T_i = 0.05$) the configuration can be less than the SQL by factors of four. The sensitivity no longer matches the slope of the SQL when the function κ is no longer constant in frequency.

TABLE I. Parameters used to model a polarization-folded speed meter. Values were chosen to correspond to Advanced LIGO [1].

Parameter	Symbol	Value	Units
Carrier laser frequency	ω_0	1.77×10^{15}	rad.s^{-1}
Mirror mass	m	40	kg
Circulating power in the cavity arms	I_0	850	kW
Arm length	L	3995	m
Arm cavity half bandwidth	γ	$T_i c/4L$	s^{-1}
Internal arm cavity transmittance	T_{i} (Power)	0.10 and 0.05	...
Output coupler mirror transmittance	T_{o} (Power)	0.72	...
Gravitational-wave frequency	Ω	10^1–10^3	s^{-1}

using parameters provided in Table I. These parameters are chosen specifically to correspond to soon-to-be-implemented Advanced LIGO parameters [1].

Speed meter operation is shown for arm cavity mirror transmissivities $T_i = 0.10$ and $T_i = 0.05$ and the parameters outlined in Table I. Figure 2 shows the two radiation coupling functions for the choices of arm cavity finesse: their function is constant below the bandwidth of the arm cavities. This is the characteristic response of a speed meter interferometer. For $|\kappa| \approx 0.7$ and $|\kappa| \approx 4.5$, the homodyne angles of 55° and 12.3° can be chosen to select a quadrature that cancels contributions from the vacuum amplitude quadrature [see Eq. (2)]. Over a broad range of frequencies below 100 Hz, the strain-referenced quantum noise floor presented in Fig. 3 shows that, with the correct choice of homodyne readout angle, contributions to quantum noise can be less than SQL by a factor of four. Outside the bandwidth of the arm cavities, the κ functions are no longer constant in frequency and no longer beat the SQL. Using the software package GWINC [14], the quantum noise contribution to the Advanced LIGO noise budget is plotted alongside the two polarization speed meter curves for comparison. Finally, it should be noted that because the gravitational-wave signal is only encoded in the phase quadrature b_2, the choice of an arbitrary readout quadrature will take projections of its magnitude onto the quadrature of choice. Thus, although quantum noise from the vacuum port are minimized, the desired signals are also reduced.

III. SPEED METER OPERATION FOR OTHER CHOICES OF WAVE PLATE ANGLE

In this section we consider the more general case where the quarter-wave plate between the Michelson and the output coupler may be oriented at any arbitrary rotation angle θ. By changing the rotation of this component, the degree of coupling between horizontal (signal) and vertical (storage) polarizations can be adjusted. A possible advantage of this tunability is that the bandwidth of the speed meter operation may be adjusted without the need to switch optics. With full rotation of the quarter-wave plate fast axis from 45° to 0°, the interferometer can be tuned from full speed meter behavior to that of a signal-recycled Michelson. This may be desirable in a future iteration of LIGO in the event that high-strain sensitivities are sought for sources in different frequency detection bands from a single detector.

Two additional quarter-wave plates oriented with their slow axis to the vertical are required for polarization tuning. In Sec. II, where the quarter-wave plate was assumed to be oriented at 45°, light was completely coupled between horizontal and vertical polarizations on reflection from the output mirror. As the wave plate is detuned from this angle, some light is reflected back into its incident polarization. On reflection from the quarter-wave plate and output coupler mirror, the vertical polarization receives a π phase flip on reflection making the vertical polarization anti-resonant. The additional wave plates—inserted on either side of the output coupler mirror—correct for this, cancelling each other's action on transmission in either direction.

In order to compute the effect of polarization coupling tuning it is necessary to modify Eqs. (6)–(9): for the more general case of arbitrary wave plate rotation θ, the new equations become

$$e_i = \sqrt{1 - T_o}\cos 2\theta f_i + \sqrt{1 - T_o}\sin 2\theta c_i + \sqrt{T_o}\cos 2\theta g_i + \sqrt{T_o}\sin 2\theta a_i, \quad (10)$$

$$d_i = \sqrt{1 - T_o}\sin 2\theta f_i + \sqrt{1 - T_o}\cos 2\theta c_i + \sqrt{T_o}\sin 2\theta g_i + \sqrt{T_o}\cos 2\theta a_i, \quad (11)$$

$$h_i = \sqrt{T_o}\cos 2\theta f_i + \sqrt{T_o}\sin 2\theta c_i - \sqrt{1 - T_o}\cos 2\theta g_i - \sqrt{1 - T_o}\sin 2\theta a_i, \quad (12)$$

$$b_i = \sqrt{T_o}\sin 2\theta f_i + \sqrt{T_o}\cos 2\theta c_i - \sqrt{1 - T_o}\sin 2\theta g_i - \sqrt{1 - T_o}\cos 2\theta a_i, \quad (13)$$

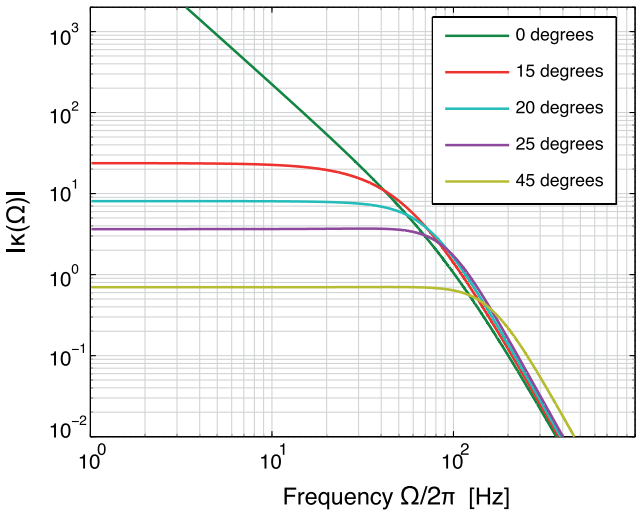

FIG. 4 (color online). Plot of radiation pressure coupling function, κ, as function of frequency for different choices of quarter-wave plate rotation θ. As the degree of wave plate rotation approaches zero degrees the bandwidth of speed meter operation narrows. The configuration approaches the behavior of signal recycling as the coupling function is no longer constant as a function of frequency. The arm cavity circulating power for these plots was adjusted to 850 kW. All other parameters are as presented in Table I.

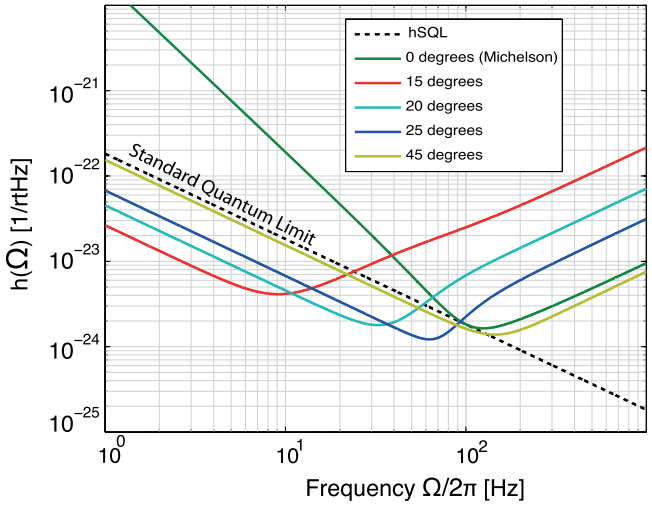

FIG. 5 (color online). Plot of gravitational strain-referenced noise sensitivity as a function of frequency for different choices of quarter-wave plate rotation θ. Corresponding to the evolution of the radiation pressure coupling function, κ (see Fig. 4), for different choices of θ sensitivities beats the standard quantum limit below the roll off of the κ function. Homodyne readout angles are chosen for each choice of θ that cancel contributions of amplitude noise obscuring the GW signal. The bandwidth of speed meter operation narrows as the degree of coupling between the polarizations is turned down (i.e., the quarter-wave plate is oriented toward zero). The arm cavity circulating power for these plots was set to 850 kW, and all other parameters are as presented in Table I.

where the output coupler mirror transmissivity is T_o and θ is the rotation of the fast axis from the horizontal.

The output quadrature fields b_i were solved in a similar manner to Sec. II B, in terms of a_i and the gravitational-wave strain signal h with the more general Eqs. (10)–(13). Using the parameters presented in Table I, with arm cavity circulating power set to 850 kW and the specific case of $T_i = 0.10$, the radiation pressure coupling functions and strain sensitivities were plotted as a function of frequency: see Figs. 4 and 5. Here the plots show an evolution of the characteristic behavior of the interferometer. As the quarter-wave plate angle is tuned away from 45°, there is a decreased degree of coupling between the polarizations and the κ function (Fig. 4) shows that the bandwidth of the signal storage and speed meter operation narrows. Conversely, the strength of coupling is increased as θ is reduced, allowing for choices of readout angle that increase the strain-equivalent performance below the SQL for the same operating power. Figure 4 shows that as θ approaches zero degrees, the interferometer approaches signal-recycled operation giving a κ response, with $1/\Omega^2$, that can only be optimized to beat the SQL at select frequencies.

Thus it follows that by rotating the wave plate the storage time of the orthogonal mode is modified, changing the bandwidth over which radiation pressure noise is suppressed. By tuning the rotation of the quarter-wave plate, the bandwidth of speed meter operation can be effectively tuned smoothly from speed meter operation to a resonant signal-recycled Michelson interferometer.

IV. IMPLEMENTING A POLARIZATION SPEED METER AND ASSOCIATED ISSUES

Figure 5 shows that the interferometer sensitivity changes smoothly as the wave-plate angle is detuned. As a consequence, the interferometer is expected to be tolerant to imperfections in wave-plate angle. A second area of potential concern relates to the polarization characteristics of the main beam splitter. Ideally the beam splitter would be 50:50 for both horizontal and vertical polarizations and produce no differential phase shift. This configuration is not expected to be sensitive to asymmetric amplitude reflectivity ($r_{bs} \neq t_{bs}$) if the second polarization is held close to a dark fringe. In this case the loss of this polarization mode by leakage towards the input laser will be minimized ($r_{bs} \times t_{bs} - t_{bs} \times r_{bs} = 0$). A differential phase shift between the two polarizations is nevertheless of concern, as this will prevent the horizontally polarized field from operating on the Michelson dark fringe, resulting in significant loss. For a beam splitting optic appropriate for use in LIGO it is anticipated that birefringence can be controlled to with 1% difference in phase between the two polarizations [15]. Careful design of the beam splitter coating or other methods to compensate for this phase may be required.

V. SUMMARY AND CONCLUSIONS

In this paper we have explored a novel implementation of a speed meter interferometer using polarization modes of an arm cavity Michelson interferometer. By modifying the topology of an advance detector such as LIGO, Virgo or KAGRA with polarization optics at its output port, it was shown that in principle such a detector could be modified to beat the standard quantum limit below 100 Hz. This presents a significant advantage over an unmodified detector, such as the Advanced LIGO, as far as quantum noise is concerned. In addition, this analysis was extended to consider the possibility of varying the degree of polarization coupling, achieved by rotating the orientation of its quarter-wave plate, as a way of tuning the speed meter operating bandwidth. As shown in Figs. 4 and 5 this tuning resulted in a smooth transition from broadband speed meter operation to signal extraction operation. This narrowing of the speed meter's bandwidth was associated with a much stronger correlation between the amplitude and phase quadrature.

As identified in the previous section, birefringence in the beam splitter is of significant concern and would be of principle technical concern for any real implementation. A more complete analysis of the polarization speed meter would include losses and injected squeezing. Finally, a feasibility survey outlining necessary polarization specifications would better inform whether this design is a realistic implementation of a generation III iteration of the LIGO interferometer.

ACKNOWLEDGMENTS

We thank Stanley E. Whitcomb and Rana Adhikari for advice and the LIGO Scientific Collaboration reviewers for improvements to this paper. We also gratefully acknowledge funding support from the Australian Research Council and the National Science Foundation under NSF Grant No. PHY-1068881 and CAREER Grant No. PHY-0956189.

APPENDIX: TWO-PHOTON FORMALISM

We analyze the dynamics of a proposed interferometer configuration using the two-photon formalism developed by Caves and Schumaker [16,17]: see Refs. [4,5,11,18] for other examples.

The two-photon formalism involves decomposing the quantized electric field into upper and lower sidebands about a carrier frequency. The fields are then factored into quadrature operators associated with the cosine and sine components of the laser carrier field. These quadrature fields are then readily propagated between optical components and used to compute the transfer of vacuum noise sources to the detector ports. To begin with, the quantized electromagnetic field, less its coherent amplitude, can be written in terms of the usual creation and annihilation operators ($a_\omega^\dagger$ and a_ω):

$$E(t) = \int_0^{+\infty} \sqrt{\frac{2\pi\hbar\omega}{\mathcal{A}c}}[a_\omega e^{-i\omega t} + a_\omega^\dagger e^{+i\omega t}]\frac{d\omega}{2\pi}, \quad \text{(A1)}$$

where the quantity $\mathcal{A}$ is the effective cross-sectional area of the beam, c is the speed of light, $\hbar$ is the reduced Planck constant and ω is the photon frequency that is integrated over to form the electric field operator E. Here the field is described for components traveling in one direction along the optic axis at a fixed point.

Gravitational waves modulate the optical path along which laser beams are propagated, resulting in phase modulation sidebands being generated from coherent light. This signal, generated as a result of the gravitational-wave strain $h(t)$, must compete with vacuum noise sidebands coupled in from open ports of the interferometer. We group vacuum noise sidebands (a_+ and a_-) pairwise corresponding to the upper and lower frequency sideband components of the gravitational-wave signal at frequency Ω. Here the sidebands are split at frequencies $\omega_0 \pm \Omega$ around the laser carrier frequency ω_0, giving annihilation operators

$$a_+ \equiv a_{\omega_0+\Omega} \quad \text{and} \quad a_- \equiv a_{\omega_0-\Omega}, \quad \text{(A2)}$$

where operator hats are omitted for notational convenience. Assuming the gravitational-wave frequency is much less than the carrier frequency ($\Omega \ll \omega_0$) the quantized electric field may be rewritten as

$$E(t) = \sqrt{\frac{2\pi\hbar\omega_0}{\mathcal{A}c}}e^{-i\omega_0 t}\int_0^{+\infty}[a_+(\Omega)e^{-i\Omega t} + a_-(\Omega)e^{i\Omega t}]\frac{d\Omega}{2\pi} + \text{H.c.}, \quad \text{(A3)}$$

where H.c. is the Hermitian conjugate. From these sidebands, quadrature fields a_1 and a_2 are defined corresponding to the cosine and sine quadratures, giving the two-photon modes defined as

$$a_1 = \frac{a_+ + a_-^\dagger}{\sqrt{2}} \quad \text{and} \quad a_2 = \frac{a_+ - a_-^\dagger}{i\sqrt{2}}. \quad \text{(A4)}$$

Thus, by factoring the electric field in terms of the cosine and sine quadratures, the field can be written as

$$E(t) = \sqrt{\frac{4\pi\hbar\omega_0}{\mathcal{A}c}}\Big[\cos(\omega_0 t)\int_0^{\infty}(a_1 e^{-i\Omega t} + a_1^\dagger e^{+i\Omega t})\frac{d\Omega}{2\pi} + \sin(\omega_0 t)\int_0^{\infty}(a_2 e^{-i\Omega t} + a_2^\dagger e^{+i\Omega t})\frac{d\Omega}{2\pi}\Big], \quad \text{(A5)}$$

or more conveniently

$$E(t) = \cos(\omega_0 t)E_1(a_1; t) + \sin(\omega_0 t)E_2(a_2; t), \quad \text{(A6)}$$

where

$$E_j(a_j;t) = \sqrt{\frac{4\pi\hbar\omega_0}{\mathcal{A}c}} \int_0^{+\infty} (a_j e^{-i\Omega t} + a_j^\dagger e^{i\Omega t}) \frac{d\Omega}{2\pi}, \quad j = 1, 2. \tag{A7}$$

The two photon formalism lends itself readily to the propagation of quantum noise, as the phase accrued during free space propagation is now decomposed into two components: a side band phase, $\phi_1 = \Omega L/c$, proportional to the side band frequency Ω, length L and speed of light c, and a carrier phase $\Phi_1 = \omega L/c$, proportional to ω, that rotates the basis of the quadratures. The evolution equations between two points q_i and q_i', in terms of carrier and side band phase accrued, are derived in Buonanno and Chen [5] and are given by

$$q_1' = e^{i\phi_1}(\cos(\Phi_1)q_1 - \sin(\Phi_1)q_2), \tag{A8}$$

$$q_2' = e^{i\phi_1}(\sin(\Phi_1)q_1 + \cos(\Phi_1)q_2). \tag{A9}$$

Thus in the form of quantized quadrature fields, quantum noise can be propagated through the interferometer from the various open ports to the read out port where their associated noise contributions can be computed.

[1] B. P. Abbott *et al.*, Rep. Prog. Phys. **72**, 076901 (2009).
[2] D. E. McClelland, N. Mavalvala, Y. Chen, and R. Schnabel, Laser Photon. Rev. **5**, 677 (2011).
[3] V. B. Braginsky and F. Ja. Khalili, Phys. Lett. A **147**, 251 (1990).
[4] H. J. Kimble, Y. Levin, A. B. Matsko, K. S. Thorne, and S. P. Vyatchanin, Phys. Rev. D **65**, 022002 (2001).
[5] A. Buonanno and Y. Chen, Phys. Rev. D **64**, 042006 (2001).
[6] J. Harms, Y. Chen, S. Chelkowski, A. Franzen, and H. Vahlbruch, Phys. Rev. D **68**, 042001 (2003).
[7] Y. Chen, Phys. Rev. D **67**, 122004 (2003).
[8] R. Schnabel, J. Harms, K. A Strain, and K. Danzmann, Classical Quantum Gravity **21**, S1045 (2004).
[9] F. Acernese *et al.*, Classical Quantum Gravity **23**, S71 (2006).
[10] K. Kuroda, *et al.*, Classical Quantum Gravity **27**, 084004 (2010).
[11] P. Purdue and Y. Chen, Phys. Rev. D **66**, 122004 (2002).
[12] S. L. Danilishin, Phys. Rev. D **69**, 102003 (2004).
[13] G. M. Harry, Classical Quantum Gravity **27**, 084006 (2010).
[14] S. Finn *et al.* GWINC-a LIGO noise calculation package, http://ilog.ligo-wa.caltech.edu:7285/advligo/gwinc.
[15] R. Lalezari (private communication).
[16] B. L. Schumaker and C. M. Caves, Phys. Rev. A **31**, 3093 (1985).
[17] C. M. Caves and B. L. Schumaker, Phys. Rev. A **31**, 3068 (1985).
[18] P. Purdue, Phys. Rev. D **66**, 022001 (2002).